Single molecule capture by a doped monatomic carbon chain

2013 J. Phys.: Condens. Matter 25 205302

(http://iopscience.iop.org/0953-8984/25/20/205302)

IOP PUBLISHING JOURNAL OF PHYSICS: CONDENSED MATTER
J. Phys.: Condens. Matter **25** (2013) 205302 (7pp) doi:10.1088/0953-8984/25/20/205302

Single molecule capture by a doped monatomic carbon chain

Zheng-Zhe Lin[1] **and Xi Chen**[2]

[1] School of Science, Xidian University, Xi'an 710071, People's Republic of China
[2] Department of Applied Physics, School of Science, Xi'an Jiaotong University, Xi'an 710049, People's Republic of China

E-mail: linzhengzhe@hotmail.com

Received 3 January 2013, in final form 7 April 2013
Published 23 April 2013
Online at stacks.iop.org/JPhysCM/25/205302

Abstract
A B-doped monatomic carbon chain has fine molecular capture ability for H_2O and especially for NO_2, which is better than that of other doped monatomic carbon chains. At 300 K and 1 atm, the capture probability of a B-doped monatomic carbon chain is appreciable even in a NO_2 concentration of 1 ppm, and the influence of the adsorbate on the quantum transport is notable for the detection. In contrast, a pure monatomic carbon chain shows its invulnerability to N_2, O_2, H_2O, NO_2, CO and CO_2, and is incapable of molecule capture due to having too low adsorption ability and weak response to quantum conductance. In the investigation of these issues, a statistic mechanical model (Lin *et al* 2011 *Europhys. Lett.* **94** 40002; 2012 *Chin. Phys. Lett.* **29** 080504) was extended to predict the adsorption and desorption rates of molecules on nanodevices. The theoretical foundation of this model was further discussed and its accuracy was verified by molecular dynamics simulations.

1. Introduction

The ideal goal of a detection method is to achieve an ultimate sensitivity such that an individual quantum can be resolved. In the case of molecular sensors, the quantum is a single atom or molecule. In order to reach this goal, a great deal of effort has been focused on solid sensors because of their high sensitivity and miniature sizes, leading to their wide use in many applications. As next-generation sensors, detectors made of low-dimensional materials have especially high sensitivity because their whole volume is exposed to adsorbates and the effect is maximized. Such detectors were first prepared using carbon nanotubes and semiconductor nanowires [1, 2], and their high sensitivity to toxic gases in very low concentrations was valuable for industrial and environmental monitoring. Then, a new detection method using single-layer graphene was developed [3]. The signal of even an individual molecule can be detected in the strong magnetic field due to the Hall effect of electrons or holes induced by the adsorbed molecules on the graphene surface acting as electronic donors or acceptors. For one-dimensional monatomic chains, the influence of adsorbates on the electronic properties may be even stronger than that for two-dimensional materials. In recent years, free-standing monatomic carbon chains (MCCs) have been carved out of single-layer graphene by a high-energy electron beam [4], or unraveled from sharp carbon specimens [5, 6] or carbon nanotubes [7], and MCCs have been predicted to be remarkably stable [8]. Recently, a mechanical procedure was proposed to prepare long pure and doped MCCs [9–11] using a nanorectifier [9] or the medium of a tunable infrared laser [12]. It was proposed that the electronic properties of MCCs could be controlled by doping a single atom or a diatomic molecule [9]. As the thinnest natural wires, MCCs should also be greatly influenced by the electronic properties of the molecules adsorbed on them.

In this work, the adsorption and desorption rates of N_2, O_2, H_2O, NO_2, CO and CO_2 on pure and doped MCCs were studied by an extension of a newly developed statistic mechanical model [8, 13], and the influence of these adsorbates on the current–voltage curves were investigated by quantum transport calculations. The pure MCC was found to be incapable of performing as a molecular capturer due to having too low adsorption ability and the weak response to quantum conductance. In contrast, the B-doped MCC has fine capture ability for H_2O and remarkably for NO_2. In the ambient of 300 K and 1 atm, the molecular capture probability is appreciable and the electric signal is notable even in a NO_2 concentration of 1 ppm.

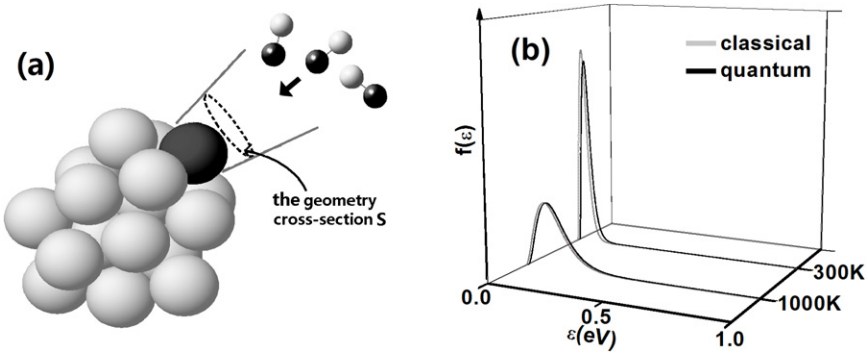

Figure 1. (a) The geometry cross-section S of the key atom in the nanodevice. (b) The kinetic energy distribution $f(\varepsilon)$ of an atom in a Cl_2 molecule at 300 and 1000 K, by classical (gray lines) and quantum mechanics (black lines), respectively.

2. Theoretical model and methodology

Generally, elementary processes correspond to some individual events in which one or two 'key atoms' cross over a static barrier E_0. For the adsorption of molecules on nanodevices, a basic event takes place when a molecule hits the nanodevice with a translational kinetic energy $\varepsilon \geq E_0$ and a specific orientation for the key atom in the molecule and the nanodevice to contact with each other. At room temperature or above, the thermal De Broglie wavelength of a molecule is at least 100 times smaller than its size, and then the molecular motion can be understood in a classical picture. By the classical ensemble theory, the distribution of molecular translational kinetic energy is Boltzmann, i.e. $f(\varepsilon) \sim \varepsilon^{1/2} e^{-\varepsilon/k_B T}$. On this basis, a simple model was built for the prediction of bimolecular chemical reaction rates [13]. Here, a similar idea was provided for predicting the molecular adsorption rate on nanodevices. By the Boltzmann distribution, the probability for the molecular translational kinetic energy $\varepsilon \geq E_0$ reads

$$P = \frac{1}{Z}\int_{E_0}^{+\infty} \varepsilon^{1/2} e^{-\varepsilon/k_B T}\, d\varepsilon, \tag{1}$$

where $Z = \int_0^{+\infty} \varepsilon^{1/2} e^{-\varepsilon/k_B T}\, d\varepsilon = \sqrt{\pi}(k_B T)^{3/2}/2$ is the partition function. Therefore, for molecules at a concentration c, the corresponding adsorption rate should be

$$\Gamma = \frac{\sigma v c}{2Z}\int_{E_0}^{+\infty} \varepsilon^{1/2} e^{-\varepsilon/k_B T}\, d\varepsilon, \tag{2}$$

where σ is the effective cross-section of the nanodevice and $v = \sqrt{2k_B T/\pi M}$ is the average thermal velocity of a molecule along the cross-section normal. The factor $1/2$ is because only half of the molecules move towards the cross-section. It should be noted that σ is not equal to the geometry cross-section S of the key atoms in the nanodevice (figure 1(a)), but instead $\sigma = S\Omega_m/4\pi$, where Ω_m is the solid angle opened by the key atom in the molecule. In practical applications, Ω_m can be estimated by the atomic distance to the molecular mass center and atomic covalent radius [13].

For the elementary processes within a system, e.g. the molecular desorption from a nanodevice, a basic event takes place when the key atom in a potential valley crosses over the barrier with a kinetic energy ε at the valley bottom larger than E_0. The atomic kinetic energy distribution is determined by $f(\varepsilon) = \sum_i f_i(\varepsilon) e^{-E_i/k_B T}/\sum_i e^{-E_i/k_B T}$, where $f_i(\varepsilon)$ is the kinetic energy distribution of the quantum state E_i. As an example, $f(\varepsilon)$ of an atom in a Cl_2 molecule is shown in figure 1(b). At room temperature or above, the distribution $f(\varepsilon)$ turns into the classical one. For a classical system including N atoms, the total energy $E = \vec{p}_1^{\,2}/2m_1 + \cdots + \vec{p}_N^{\,2}/2m_N + V(\vec{x}_1, \ldots, \vec{x}_N)$ and the kinetic energy distribution of the ith atom reads

$$\begin{aligned} f(\varepsilon) &= \int \delta[\vec{p}_i^{\,2}/2m_i - \varepsilon] e^{-E/k_B T}\, d\vec{p}_1 \ldots d\vec{p}_N\, d\vec{x}_1 \\ &\quad \ldots d\vec{x}_N \Big/ \int e^{-E/k_B T}\, d\vec{p}_1 \ldots d\vec{p}_N\, d\vec{x}_1 \ldots d\vec{x}_N \\ &= \int \delta[\vec{p}_i^{\,2}/2m_i - \varepsilon] \\ &\quad \times e^{-\vec{p}_i^{\,2}/2m_i k_B T}\, d\vec{p}_i \Big/ \int e^{-\vec{p}_i^{\,2}/2m_i k_B T}\, d\vec{p}_i \\ &= \varepsilon^{1/2} e^{-\varepsilon/k_B T}/Z. \end{aligned} \tag{3}$$

This Boltzmann distribution for the atomic kinetic energy is in very good agreement with MD simulations [8]. In most cases, the atomic kinetic energy ($\sim k_B T$) at the valley bottom is significantly smaller than E_0, and the atom vibrates many times within the valley before crossing over the barrier. With a vibration frequency Γ_0, the rate for the atomic event reads

$$\Gamma = \frac{\Gamma_0}{Z}\int_{E_0}^{+\infty} \varepsilon^{1/2} e^{-\varepsilon/k_B T}\, d\varepsilon. \tag{4}$$

For a given ε, the oscillation period $\tau(\varepsilon) = \sqrt{m}\int d\vec{x}\,/\,2[\varepsilon - V(\vec{x})]$ along the minimum energy path (MEP) can be determined by $V(\vec{x}) = \int \vec{F}(\vec{x}) \cdot d\vec{x}$, where $\vec{F}(\vec{x})$ is the force felt by the key atom at position $\vec{x}$ [8]. With the corresponding oscillation frequency $\nu(\varepsilon) = 1/\tau(\varepsilon)$, the averaged frequency reads

$$\Gamma_0 = \frac{\int_0^{E_0} \nu(\varepsilon)\varepsilon^{1/2} e^{-\varepsilon/k_B T}\, d\varepsilon}{\int_0^{E_0} \varepsilon^{1/2} e^{-\varepsilon/k_B T}\, d\varepsilon}. \tag{5}$$

For two-key-atom processes, an event takes place when the atomic kinetic energy sum $\varepsilon_1 + \varepsilon_2 \geq E_0$, and the

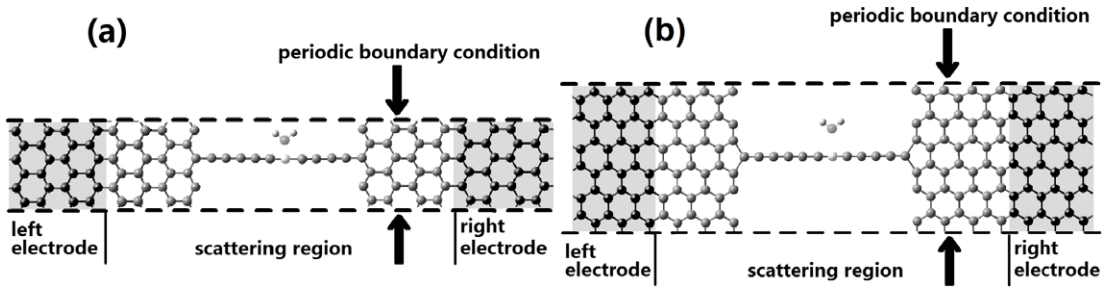

Figure 2. The simulation system of a pure or doped MCC of ten atoms bridged between two graphene lattices in the armchair (a) or zigzag (b) orientation, with the atoms shown in black fixed.

corresponding rate should be

$$\Gamma = \frac{\Gamma_0}{Z^2}\iint_{\varepsilon_1+\varepsilon_2\geq E_0} \varepsilon_1^{1/2}\varepsilon_2^{1/2}\mathrm{e}^{-(\varepsilon_1+\varepsilon_2)/k_\mathrm{B}T}\,\mathrm{d}\varepsilon_1\,\mathrm{d}\varepsilon_2$$
$$= \frac{\Gamma_0}{2(k_\mathrm{B}T)^3}\int_{E_0}^{+\infty}\varepsilon^2\mathrm{e}^{-\varepsilon/k_\mathrm{B}T}\,\mathrm{d}\varepsilon. \quad (6)$$

In our previous work [8], equations (4) and (6) were verified by MD simulations and successfully applied to predict the stability of an MCC–graphene junction and bonds in the MCC body, producing results in good agreement with the experimental data.

To investigate the molecular adsorption and desorption rates on MCCs, *ab initio* calculations were performed for a ten-atom pure or doped MCC bridged between two graphene lattices in the armchair (figure 2(a)) or zigzag (figure 2(b)) orientation with the atoms shown in black fixed. Simulations were carried out for pure, B-doped, N-doped and BN-doped MCCs coupling with N_2, O_2, H_2O, NO_2, CO and CO_2 molecules. The geometry optimizations, reaction barriers E_0, MEPs and forces $F(\vec{x})$ felt by the key atom were calculated using the pseudoreaction coordinate method on the level of density functional theory (DFT) via the Gaussian 03 package [14] with the 6-31G(d, p) basic set and the newly developed hybrid X3LYP functional including dispersion interactions [15], which is considered to be more accurate than other functionals in potential surface and MEP calculations. Canonical modes for the geometries of potential minima and transition states were calculated to confirm the optimization results.

For quantum transport, the simulation system was set up by appending semi-infinite graphene electrodes in the armchair (figure 2(a)) or zigzag (figure 2(b)) orientation to the two terminals of the pure or doped MCC, with or without the adsorbed molecule. Calculations were performed by the TRANSIESTA package [16], using a non-equilibrium Green's function [17] at the level of the Perdew–Burke–Ernzerhof parameterized generalized-gradient approximation [18] with the Troullier–Martins pseudopotential [19] and a localized double-zeta polarized basis set in order to preserve a correct description of π-conjugated bonds. The mesh cutoff energy was 150 Ryd, and a k-point sampling of $1 \times 8 \times 100$ was used. For a bias voltage V_b applied on the electrodes, the current is given by the Landauer–Büttiker equation [16]

$$I = \frac{2e}{h}\int T(E, V_\mathrm{b})\left[f_L\left(E - E_\mathrm{F} - \frac{eV_\mathrm{b}}{2}\right)\right.$$
$$\left. - f_R\left(E - E_\mathrm{F} + \frac{eV_\mathrm{b}}{2}\right)\right]\mathrm{d}E, \quad (7)$$

where $T(E, V_\mathrm{b})$ is the scattering coefficient of the band state at energy E, E_F is the Fermi energy of the electrodes and f_L and f_R are the Fermi–Dirac distribution functions of the two electrodes, respectively. As buffer layers, sufficient graphene lattices in the scattering region are essential to screen the induced electric field between the two electrodes. Our calculations showed that the transport properties do not change appreciably when there are at least two buffer layers for the armchair orientation, or three for the zigzag orientation.

3. Results and discussion

3.1. MD simulation

To verify equation (2), molecular dynamics (MD) simulations were performed for molecular adsorption on a monatomic chain. The simulation system was set up by placing a 20-atom MCC with its terminals fixed and 33 helium atoms as the buffer gas (BG) along with a diatomic molecule initialized in a random position in a periodic cubic box with a side length of 30 Å. The BG atoms were controlled by a thermal bath at temperature T. The Brenner potential [20, 21] was applied for C–C interactions, and the interaction between the atoms of the diatomic molecule reads

$$V_{mm}(r) = C_1\mathrm{e}^{C_2 r} - C_3\mathrm{e}^{-C_4 r}, \quad (8)$$

with a bond energy of 1.05 eV ($C_1 = 9.073 \times 10^5$ eV, $C_2 = 10.925$ Å^{-1}, $C_3 = 3.514$ eV and $C_4 = 0.764$ Å^{-1}). A modified Lennard-Jones potential

$$V_{cm}(r) = D_1/r^{12} - D_2/r^6 + D_3/r^3 \quad (9)$$

was designed for the interaction between C and the atoms of the diatomic molecule ($D_1 = 3.028 \times 10^3$ eV Å^{12}, $D_2 = 3.177 \times 10^2$ eV Å^6 and $D_3 = 33.348$ eV Å^3), providing an adsorption barrier $E_{0\mathrm{a}} = 1.052$ eV. These parameters for the artificially constructed potential equations (8) and (9) were

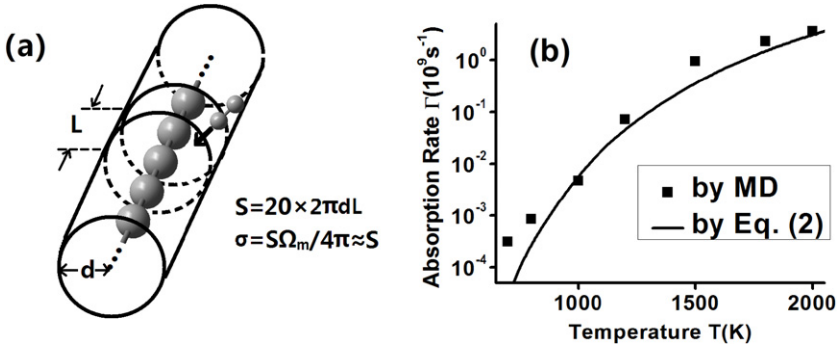

Figure 3. The cross-section σ for the adsorption of a molecule (a) described by the artificially constructed potential equations (8) and (9), and the corresponding adsorption rate (b) on a 20-atom MCC.

Table 1. The adsorption and desorption barriers of some molecules against a pure MCC, in which '—' means unable to be adsorbed.

	NO_2	CO	CO_2	N_2	H_2O	O_2
Adsorption barrier E_{0a} (eV)	0	0	0	—	—	0.93
Desorption barrier E_{0d} (eV)	0.024	0.017	0.028	—	—	0.38

adjusted to let the adsorption and desorption occur within the time scale of MD simulations. Because our model does not depend on the specific form of the interaction potential, it is suitable for the adsorption and desorption progress of any diatomic molecule on a monatomic chain, and the chosen parameters for equations (8) and (9) do not affect the verification of the model. For $T = 700$–2000 K, the average time for one event is in the range of several μs to several hundreds of ps, and simulations were performed repeatedly at every temperature until the average adsorption rate changed by less than 5% (about 10 times for low temperature and 10^3 times for high temperature). The geometry cross-section σ of the 20-atom MCC is estimated as $S = 20 \times 2\pi dL = 1101.07$ Å^2, where $d = 6.74$ Å is the distance from the molecular mass center to the MCC axis where the barrier E_0 appears, and $L = 1.30$ Å is the C–C bond length in the MCC (figure 3(a)). For a diatomic molecule, the solid angle taken by an atom in the molecule gets close to 2π, and for the two atoms $\sigma = S\Omega_m/4\pi \approx S$. From the results, the adsorption rates predicted by equation (2) are in good agreement with MD (figure 3(b)). It is worth noting that the model is also applicable to triatomic or polyatomic molecules because equation (2) is independent of the molecular geometry.

3.2. DFT calculation for a pure MCC

Along the MEPs of NO_2, CO and CO_2 molecules approaching a pure MCC, the potential drops to a valley of 0.017–0.028 eV without barriers, while only repulsive interactions were found for N_2 and H_2O (table 1). The molecular coverage of the MCC is estimated as follows. For the barrierless adsorptions, equation (2) becomes $\Gamma_a = \sigma vc/2$. The desorption event takes place when the bond between the MCC and the molecule breaks, i.e. the kinetic energy sum $\varepsilon_1 + \varepsilon_2$ of the two bonding atoms is larger than E_0, and equation (6) should be applied. The molecule can go away from the MCC along the radial direction and two tangential directions perpendicular to the chain axis, and, indeed, three equivalent paths were found in the MEP calculations. In the NO_2 ambient of 300 K and 1 atm, by $\sigma \approx 28.0$ Å^2 the molecular adsorption rate on one C atom is about $\Gamma_a = 6.4 \times 10^8$ s^{-1}. By $E_{0d} = 0.024$ eV and $\Gamma_0 = 1.0 \times 10^{12}$ s^{-1}, the corresponding desorption rate is estimated to be $\Gamma_d = 2.8 \times 10^{12}$ s^{-1}, and so in equilibrium the ratio of C atoms covered by NO_2 molecules is $R = \Gamma_a/(\Gamma_a + \Gamma_d) \approx 0.02\%$. At 1000 K, the ratio even decreases to $R \approx 0.01\%$. Such weak interaction presents the invulnerability of MCCs to these molecules, and they have little influence on the quantum transport. The I–V_b curves are shown in figures 4(a) and (b), for the graphene electrodes in the armchair and zigzag orientations, respectively. Similar situations are also found for CO and CO_2. Such small molecular coverage probability and small difference of the I–V_b curve between a solo MCC and an MCC with an adsorbed molecule means that a pure MCC could not be used as a capturer or detector for these molecules.

For the O_2 molecule, barriers of $E_{0a} = 0.93$ eV for the adsorption and $E_{0d} = 0.38$ eV for the desorption (table 1) were found in the MEP calculation (figure 4(c)), respectively, corresponding to adsorption and desorption rates much slower than those in NO_2, CO and CO_2 due to these barriers. In the ambient of 1 atm O_2 at 300 K, it takes $\tau_a = 1/\Gamma_a = 222$ h and $\tau_d = 1/\Gamma_d = 346$ h for a C atom to capture and release one O_2 molecule, respectively (figure 4(d)). Note that although $E_{0a} > E_{0d}$, the adsorption time τ_a is shorter than the desorption time τ_d because of the high O_2 concentration c. In equilibrium the coverage ratio of O_2 on the MCC is up to $R = \Gamma_a/(\Gamma_a + \Gamma_d) \approx 60.9\%$. However, such status cannot be achieved in a short time due to too long τ_a and τ_d. At higher temperature, τ_a becomes much shorter than τ_d by orders of magnitude, and so the coverage of O_2 sharply increases. For example, at 400 K it takes $\tau_a = 132$ s for a C atom to capture an O_2, but $\tau_d = 15$ h for the release process (figure 4(d)). In this case, the MCC will be rapidly oxidized because the coverage of O_2 becomes

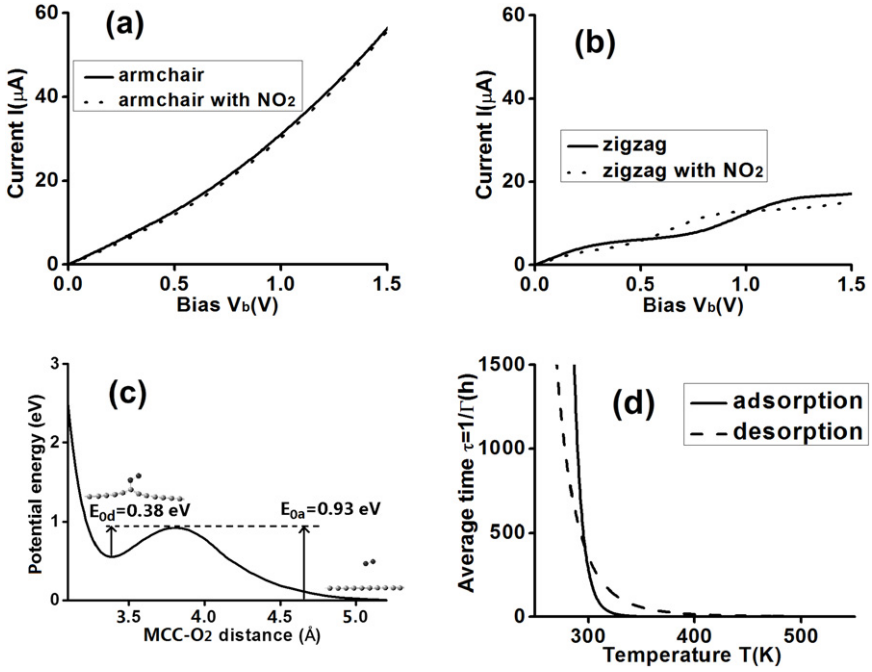

Figure 4. The I–V_b curves for a solo MCC and an MCC with an adsorbed NO_2 molecule, with the graphene electrodes in the armchair (a) or zigzag (b) orientation. The potential energy profile along the MEP with the changing distance from the O_2 mass center to the MCC axis (c). The average time $\tau = 1/\Gamma$ taken for a C atom in the MCC to capture (solid line) or release (dashed line) a molecule in the ambient of 1 atm O_2 (d).

Table 2. The adsorption and desorption barriers of some molecules against a B-doped MCC.

	NO_2	CO	CO_2	N_2	H_2O
Adsorption barrier E_{0a} (eV)	0	0	0	0	0.75
Desorption barrier E_{0d} (eV)	1.27	0.001	0.012	0.021	1.12

$R = \Gamma_a/(\Gamma_a + \Gamma_d) \approx 99.8\%$. Therefore, a pure MCC is not suitable for O_2 capture either at room temperature or at higher temperature.

3.3. DFT calculation for B- and N-doped MCCs

The molecular adsorption ability could be enhanced by doping one B atom in the MCC because of the bonding by the injecting electrons of the molecule to the empty orbital of the B atom. According to the result, such bonding was found for H_2O and NO_2 molecules. For H_2O, the unshared pair of electrons on the O-atom couples with the B atom, providing an adsorption barrier $E_{0a} = 0.75$ eV and a desorption barrier $E_{0d} = 1.12$ eV (table 2). For a longer MCC, E_{0a} becomes a little lower. At the saturated vapor pressure of H_2O at 300 K (3.6 kPa, corresponding to a concentration of 1.4×10^{-3} mol l^{-1}), it takes $\tau_a = 1/\Gamma_a = 3.7$ h for the B atom to capture an H_2O molecule, and the H_2O molecule stays on the B atom for $\tau_d = 1/\Gamma_d = 12$ min, which is long enough for detection of the captured molecule (figure 5(a)). Although $E_{0a} < E_{0d}$, τ_a is longer than τ_d due to the low H_2O concentration c. At higher temperature, although the time τ_a for the capture is much shorter, detection becomes unfeasible because τ_d decreases by orders of magnitude and the captured molecule cannot stay for an appreciable time. For example, at 400 K it takes $\tau_a = 13$ s for one capture, but the H_2O molecule only stays for $\tau_d = 26$ ms on the B atom. When the temperature is below 250 K, τ_a becomes much larger than that at 300 K by orders of magnitude, indicating that the molecule capture event can hardly occur at low temperature. Therefore, the B-doped MCC could be an H_2O capturer only at a temperature near 300 K. For quantum transport, the adsorption of H_2O leads to an obvious reduction in the current I for the graphene electrodes, no matter whether they are in the armchair (figure 5(c)) or zigzag (figure 5(d)) orientation, which acts as a notable detectable signal of the B-doped MCC capturing an H_2O molecule.

The adsorption of NO_2, CO, CO_2 and N_2 molecules on the B atom of the doped MCC was found to be barrierless (table 2). For CO, CO_2 and N_2, the adsorbed molecule leaves the MCC quickly with a high rate Γ_d because of too small E_{0d}. For NO_2, the corresponding adsorption rate $\Gamma_a = \sigma vc/2$ is much faster than that of H_2O by orders of magnitude. In the NO_2 ambient of 1 atm and the temperature range of $T = 300$–1000 K, the time $\tau_a = 1/\Gamma_a = 2\times10^{-3}$–$3\times10^{-3}$ μs means that the adsorption of NO_2 on the B atom takes place quickly. The desorption barrier, i.e. the adsorption energy, was found to be $E_{0d} = 1.27$ eV. At 300 K, the time $\tau_d = 1/\Gamma_d = 20$ h for which the captured NO_2 molecule stays on the B atom means that the molecule can hardly escape (figure 5(b)).

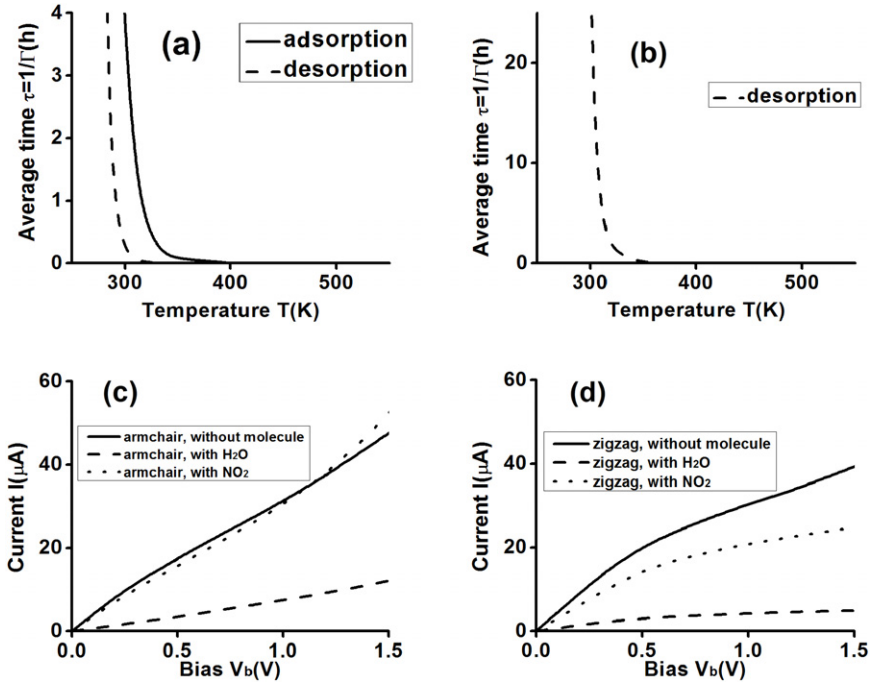

Figure 5. The average time $\tau = 1/\Gamma$ taken for the B atom in the doped MCC to capture a molecule in an H_2O vapor of 3.6 kPa (solid line), or to release an adsorbed H_2O molecule (dashed line) (a); τ for the B atom releasing an adsorbed NO_2 molecule (b). The I–V_b curves for a solo B-doped MCC or a B-doped MCC with an adsorbed H_2O or NO_2 molecule on the B atom, with the graphene electrodes in the armchair (c) or zigzag (d) orientation.

τ_d decreases with increasing temperature (figure 5(b)), and the desorption event, i.e. $\tau_d \ll \tau_a$, occurs at temperatures above 1000 K. At 300 K and 1 atm, even when the NO_2 concentration decreases to 1 ppm (i.e. a partial pressure of 0.1 Pa), the time $\tau_a = 1.9$ ms to capture an NO_2 molecule is still short. Therefore, the B-doped MCC should be a very good capturer for NO_2 even in very low concentration. However, notable reduction in the quantum transport current I was only found for the graphene electrodes in the zigzag orientation (figure 5(d)), while no obvious change in the I–V_b curve was found for the armchair one (figure 5(c)).

An MCC doped by an N atom or a BN diatomic molecule has much lower molecule capture ability than the B-doped MCC. The desorption barrier E_{0d} is in the range of 0.1–0.4 eV for a captured H_2O or NO_2 molecule to leave an N-doped or BN-doped MCC, while repulsive interactions were found for N_2, CO and CO_2. Such low E_{0d} corresponds to a very small τ_d of the order of magnitude of 10^{-7}–10^{-3} μs at room temperature, indicating that the N-doped and BN-doped MCCs could not be used as molecular capturers.

3.4. Conditions for a good molecular capturer

A good molecular capturer should have a short molecular adsorption time $\tau_a = 1/\Gamma_a$ and a long desorption time $\tau_d = 1/\Gamma_d$. For general molecules, the molecular mass and collision cross-section with one atom in the monatomic chain could be roughly estimated as $M \approx 10$–50 amu and $\sigma \approx 10$–50 Å^2, respectively, and by equation (5) Γ_0 generally has a value in the range of 10^{13}–10^{14} s^{-1}. Therefore, τ_a and τ_d can be estimated by equations (2) and (6). At 300 K, in the 1 atm ambient of the molecule τ_a is less than several hours if $E_{0a} < 0.8$ eV, and τ_d is longer than dozens of minutes if $E_{0d} > 1.1$ eV. For a B-doped MCC, the H_2O molecule against the B atom just fits this condition, and the NO_2 molecule could be well captured by the B atom because $E_{0a} = 0$ and the E_{0d} is larger than that of H_2O. In contrast, a pure or N-doped MCC could not be a good molecular capturer due to too low E_{0d}.

4. Summary

In this work, a statistic mechanical model [8, 13] was extended to the predict the adsorption and desorption rates of small molecules on nanodevices. This model is based on the fact that the kinetic energy distribution of atoms or molecules always obeys $\varepsilon^{1/2}e^{-\varepsilon/k_BT}$, and its theoretical foundation was further investigated. The accuracy of the corresponding extension was verified by MD simulations. By *ab initio* calculations, the extended model was applied to prediction of the adsorption and desorption rates of N_2, O_2, H_2O, NO_2, CO and CO_2 on pure and doped MCCs. From the results, a pure MCC is incapable of being a molecular capturer due to low adsorption probability for N_2, H_2O, NO_2, CO and CO_2 molecules at room temperature, and the influence of these molecules on the current–voltage curves is weak due to the poor adsorption. For O_2, at room temperature the corresponding adsorption rate is too slow, while at higher temperature the MCC will be rapidly oxidized. In contrast, a B-doped MCC has fine capture ability for H_2O and remarkably for NO_2, which is better than that of N-doped or BN-doped MCCs, and the

reduction of the quantum transport current by the captured molecule is notable, which could be a detectable electronic signal of the molecule capture. At room temperature and 1 atm, even in a NO_2 concentration of 1 ppm, the change in the current–voltage curves of the B-doped MCC is appreciable and the captured NO_2 could stay for a long time on the B atom, indicating that the B-doped MCC could be a very good single molecule capturer and detector for NO_2.

Acknowledgment

This work was supported by the Fundamental Research Funds for the Central Universities.

References

[1] Kong J, Franklin N R, Zhou C, Chapline M G, Peng S, Cho K and Dai H 2000 *Science* **287** 622
[2] Collins P G, Bradley K, Ishigami M and Zettl A 2000 *Science* **287** 1801
[3] Schedin F, Geim A K, Morozov S V, Hill E W, Blake P, Katsnelson M I and Novoselov K S 2007 *Nature* **6** 662
[4] Jin C, Lan H, Peng L, Suenaga K and Iijima S 2009 *Phys. Rev. Lett.* **102** 205501
[5] Mikhailovskij I M, Wanderka N, Ksenofontov V A, Mazilova T I, Sadanov E V and Velicodnaja O A 2007 *Nanotechnology* **18** 475705
[6] Mazilova T I, Mikhailovskij I M, Ksenofontov V A and Sadanov E V 2009 *Nano Lett.* **9** 774
[7] Börrnert F *et al* 2010 *Phys. Rev.* B **81** 085439
[8] Lin Z-Z, Yu W-F, Wang Y and Ning X-J 2011 *Europhys. Lett.* **94** 40002
[9] Lin Z-Z and Ning X-J 2011 *Europhys. Lett.* **95** 47012
[10] Wang Y, Lin Z-Z, Zhang W, Zhuang J and Ning X-J 2009 *Phys. Rev.* B **80** 233403
[11] Wang Y, Ning X-J, Lin Z-Z, Li P and Zhuang J 2007 *Phys. Rev.* B **76** 165423
[12] Lin Z-Z, Zhuang J and Ning X-J 2012 *Europhys. Lett.* **97** 27006
[13] Li W-Y, Lin Z-Z, Xu J-J and Ning X-J 2012 *Chin. Phys. Lett.* **29** 080504
[14] Frisch M J *et al* 2003 *Gaussian 03, Revision B.04* (Pittsburgh, PA: Gaussian, Inc.)
[15] Xu X and Goddard W A 2004 *Proc. Natl Acad. Sci.* **101** 2673
[16] Büttiker M, Imry Y, Landauer R and Pinhas S 1985 *Phys. Rev.* B **31** 6207
[17] Taylor J, Guo H and Wang J 2001 *Phys. Rev.* B **63** 245407
[18] Perdew J P, Burke K and Ernzerhof M 1996 *Phys. Rev. Lett.* **77** 3865
[19] Troullier N and Martins J L 1991 *Phys. Rev.* B **43** 1993
[20] Brenner D W 1990 *Phys. Rev.* B **42** 9458
[21] Halicioglu T 1991 *Chem. Phys. Lett.* **179** 159